Journal of the Korean Physical Society, Vol. 66, No. 1, January 2015, pp. 117∼122

Raman Scattering Studies of Cu_2ZnSnS_4 Thin Films: Local Distribution of the Secondary Phase $Cu_{2-x}S$ and the Effect of KCN Etching on $Cu_{2-x}S$

Trang Thi Thu Nguyen, Hae-Young Shin, Gee Yeong Kim, Ju Ri Kim, William Jo and Seokhyun Yoon*
Department of Physics, Ewha Womans University, Seoul 120-750, Korea

Ki Doo Lee and Jin Young Kim
Photo-electronic Hybrids Research Center, Korea Institute of Science and Technology (KIST), Seoul 136-791, Korea

(Received 8 December 2013, in final form 20 February 2014)

We used X-ray diffraction (XRD) and Raman scattering spectroscopy to study Cu_2ZnSnS_4 (CZTS) thin films grown by using an electroplating method. We compared the Raman spectra of the CZTS thin films before and after potassium cyanide (KCN) etching. We observed a phonon mode of the secondary phase $Cu_{2-x}S$ both from Cu-rich and Cu-poor CZTS samples before the KCN etching. We found that the intensity of the $Cu_{2-x}S$-related vibration mode depended on the excitation wavelength, from which we could estimate the stoichiometry of the $Cu_{2-x}S$ as $x = 1$. Interestingly, the $Cu_{2-x}S$ phonon is completely removed after the KCN etching. We could also get information regarding the local distribution of the secondary phase on the surfaces of the CZTS thin films by using micro-Raman scattering spectroscopy.

PACS numbers: 42.79.-e, 78.30.-j, 78.66.Db
Keywords: CZTS, Raman scattering spectroscopy, Electroplating, KCN etching, Secondary phase
DOI: 10.3938/jkps.66.117

I. INTRODUCTION

In recent years, $Cu_2ZnSn(S,Se)_4$ (CZTSSe) has drawn much attention as one of the most promising absorber layer materials for low-cost thin-film solar cells and has been studied as a substitute for $Cu_2ZnSn(S,Se)_4$ (CIGS). The efficiency of CZTSSe thin-film solar cells has reached 12.6% [1]. In particular, CZTS is regarded as an ideal absorption material due to its p-type conductivity, 1.5-eV direct band gap, and high optical absorption coefficient ($\alpha > 10^4$ cm^{-1}) [2]. The highest conversion efficiency for CZTS is 8.4% [3], which is much lower than that of CIGS photovoltaic devices (∼20%) [4].

One important aspect to get high efficiency while characterizing CZTS cells is to clarify the growth mechanism of the thin films. Many methods, such as thermal evaporation [3,5], atom beam sputtering [6], spray pyrolysis [7], pulsed laser deposition [8], electroplating [9,10] and other vacuum and non-vacuum processes, can be used to grow CZTS thin films for use as an absorber layer material. The highest conversion efficiency for CZTS thin films grown by electrodepositing is 7.3% [11]. For comparison, the highest conversion efficiencies are 8.4% [3] and 6.8% [6] for films grown by using thermal coevaporation and sputtering, respectively. In the future, the electroplating method would be preferred because it can provide a high-quality film at a very low cost. It also has merits, such as its being a high-rate process, its using very low-cost starting materials, and so on [12]. However, most of the electrochemical deposition techniques reported so far produced stacked film of Cu, Sn and Zn layers that were subsequently annealed under a sulfur atmosphere which could lead to the formation of secondary phases [13]. To overcome this disadvantage, KCN etching has been used to remove the second phases related with the Cu-rich layers for solar-cell thin films [14–16].

In this research, we used X-ray diffraction (XRD) and Raman scattering spectroscopy to investigate the deformation of the composition distribution of unetched and etched CZTS thin films grown by using the electroplating method by using. XRD is commonly used for the structural analysis of polycrystalline thin-films. However, in the case of CZTS, several secondary phases exist, so XRD alone is not sufficient to resolve the phases that may be present [11,17]. Thus, we performed a useful complementary tool of Raman scattering spectroscopy to distinguish the CZTS from the secondary phases and to study them locally.

*E-mail: syoon@ewha.ac.kr; Fax: +82- 2-3277-2372

Table 1. Chemical compositional ratio of the thin films.

	Compositional ratio (%)	
	Cu/(Zn+Sn)	Zn/Sn
Cu-poor	0.79	1.55
Cu-rich	1.89	1.56

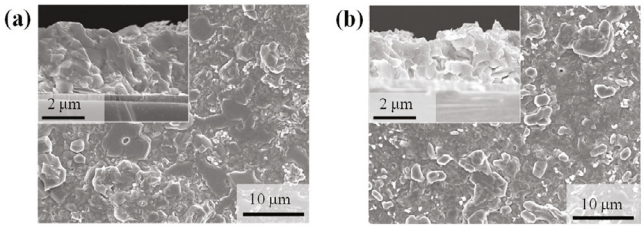

Fig. 1. Plane and cross-sectional SEM images of CZTS with different precursor: (a) Cu/(Zn+Sn) = 0.79 and Zn/Sn = 1.55 and (b) Cu/(Zn+Sn) = 1.89, Zn/Sn = 1.56.

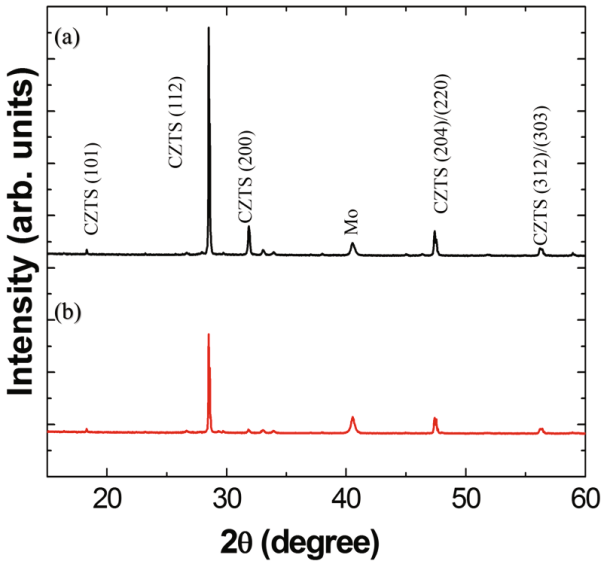

Fig. 2. (Color online) X-ray diffraction spectra of (a) Cu-poor sample and (b) Cu-rich sample CZTS thin films electroplated on Mo/SLG substrates.

II. EXPERIMENTS

CZTS thin films were grown by using an electroplating deposition process, which is a non-vacuum method. Cu-Zn-Sn metallic precursor layers were coated on Mo/soda-lime glass by using a potentiostat (model: WPG100, Won-A Tech, Korea) from an aqueous solution containing Cu, Zn, and Sn ions. The molar concentrations of the starting materials are 0.02 M for $CuSO_4{\cdot}5H_2O$, 0.035 M for $ZnSO_4{\cdot}7H_2O$, 0.014 M for $SnCl_2$, and 0.5 M for tri-sodium citrate [18]. The raw materials were deposited under a constant current density of -1.3 mA/cm^2 for 2000 s. A three-electrode system was applied for coating Mo on the glass, a Pt plate (counter), and a saturated Ag/AgCl reference electrode. The precursor films were annealed at 550 °C in a quartz tube furnace under a sulfur atmosphere (vaporized elemental sulfur with a high-purity Ar carrier gas) [16]. Lee *et al.* reported that the conversion of efficiency of the grown CZTS thin-film solar cells was about 2% [19]. The surface morphologies and the chemical compositions of the CZTS films were examined using scanning electron microscopy (SEM) and energy dispersive spectrometry (EDS), respectively.

The crystal structures of the CZTS thin-films were examined by using X-ray diffraction (Bruker, New D8 Advance with a CuKα radiation source, $\lambda = 1.5106$ Å, 4 °/min scan speed) from 10 to 90°. Macro-Raman and micro-Raman spectra were measured by using a McPherson 207 spectrometer equipped with a nitrogen-cooled charge-coupled-device (CCD) array detector. CZTS films were excited with a 632.8-nm He-Ne laser and a 488-nm diode laser focused to a ∼100-μm-diameter spot in the macro Raman measurements and to an ∼1-μm-diameter spot by using a microscope objective (×100) in the micro Raman measurements.

KCN is the formula of a potassium-cyanide compound and is produced by treating hydrogen cyanide with a 50% aqueous solution of potassium hydroxide, followed by evaporation of the solution in a vacuum [20,21]. For chalcopyrite and kesterite thin-film absorbers, KCN has been used to effectively remove secondary phases of chalcogen compounds with Cu, Zn, and Sn [14–16,22,23]. In order to observe the effects of KCN on the secondary phases in the CZTS thin films, we dipped the samples in a 10% KCN solution for 3 minutes at room temperature.

III. RESULTS AND DISCUSSION

Table 1 shows chemical compositional ratios for the Cu-poor (Cu/(Zn + Sn) = 0.79) and the Cu-rich [Cu/(Zn + Sn) = 1.89] CZTS thin films that we measured. Figure 1 displays plane and cross-sectional SEM images of the CZTS thin films. Grains of both of the films are seen to be grown well, and average size is larger than 2 μm. The thickness of the CZTS films is about 3.5 m. The XRD diffractograms of the samples are shown in Fig. 2. The major diffraction peaks appear at $2\theta = 28.5$, 33, 47.4, and 56.3°, which are assigned to be the (112), (200), (220), and (312) reflections of CZTS [8,24]. No diffraction peaks of secondary phases related with $Cu_{2-x}S$ ($x = 1$) [25] are clearly observed.

Figure 3 illustrates the macro-Raman spectra of the Cu-poor and the Cu-rich samples excited with a 488-nm laser and a 632.8-nm laser. One strong and two weak CZTS-related peaks are observed from both samples: The strong mode (A_1) at 337 cm^{-1} is associated with vibrations of S atoms [26]. A weak mode (A) is

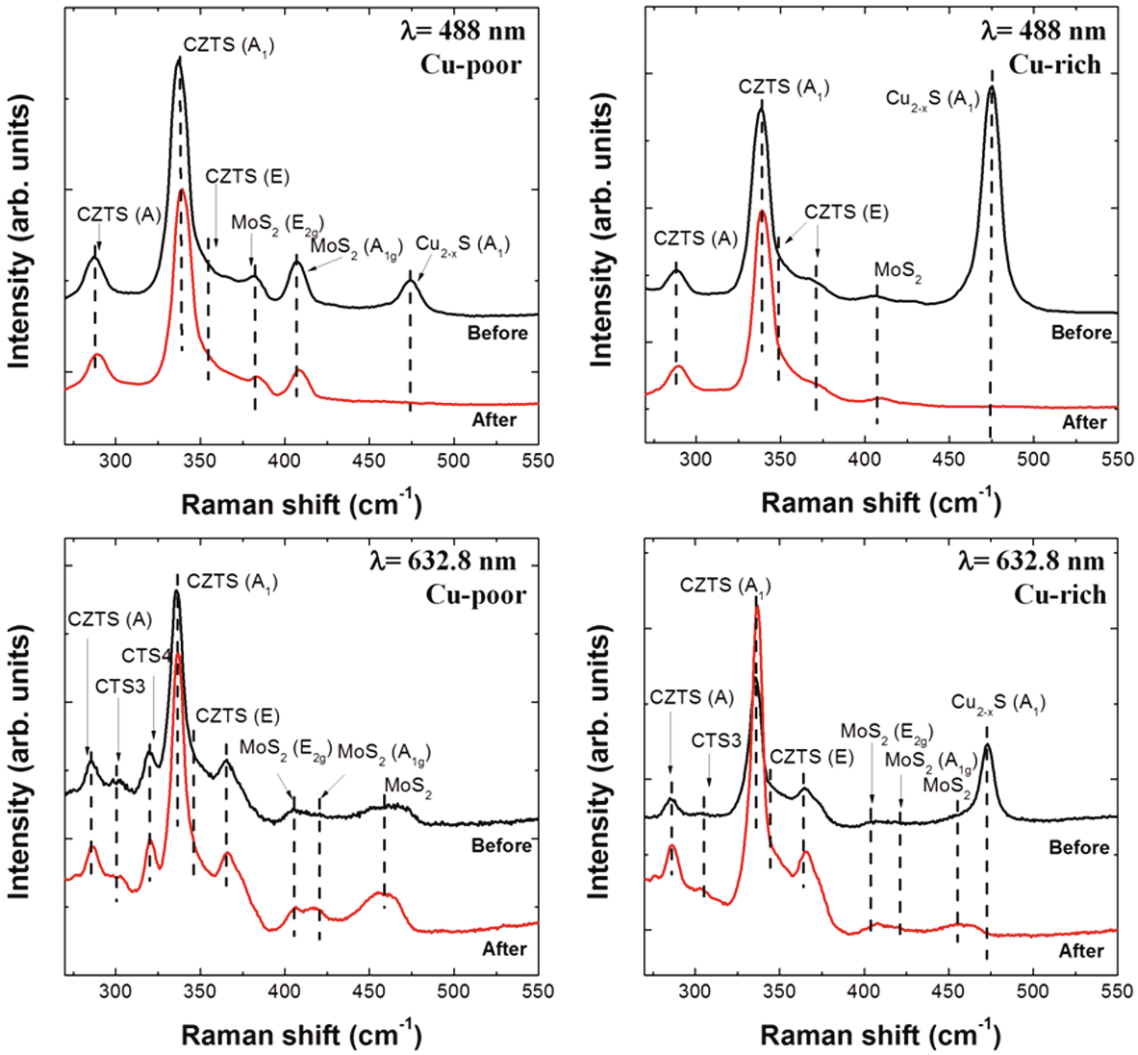

Fig. 3. (Color online) Macro-Raman spectroscopy results for CZTS (a, c) Cu-poor and (b, d) Cu-rich thin films before KCN-etching (black line) and after KCN-etching (red line) by using a 488-nm laser and a 632.8-nm laser.

seen at 287 cm^{-1}, and a shoulder peak is observed at 364 cm^{-1} (E) [27]. The sharpness and the strong intensity of the CZTS mode suggest that the crystalline quality of the films is good. Two MoS_2 Raman modes, one at 381 cm^{-1} and the other at 408 cm^{-1}, are observed from Cu-poor (Cu-rich) samples under 488-nm laser excitation, as shown in Fig. 3(a). A Raman mode of $Cu_{2-x}S$ is clearly seen at 473 cm^{-1} (A_1 (LO) mode) [28] before the KCN etching. The peak frequency of the $Cu_{2-x}S$ mode is known to depend on x, and the energy of 473 cm^{-1} is assigned to the S-S stretching mode of $Cu_{2-x}S$ with $x = 1$ [29]. Interestingly, the $Cu_{2-x}S$ mode completely disappears after the KCN etching, as shown in Fig. 3(a). In the Cu-rich sample, a $Cu_{2-x}S$ mode is observed at ∼475 cm^{-1} before the KCN etching and the peak intensity is even stronger than that of the CZTS A_1 mode at 337 cm^{-1} (Fig. 3(b)), which indicates that the $Cu_{2-x}S$ compound is more abundant in Cu-rich samples than in Cu-poor samples and that the $Cu_{2-x}S$ mode completely disappears after the a Cu-rich sample is etched with KCN.

Figures 3(c) and (d) show the Raman spectra of Cu-poor and Cu-rich samples excited with a 632.8-nm laser. For the Cu-poor sample, CZTS, Cu_2SnS_3 (CTS3), Cu_3SnS_4 (CTS4) and MoS_2 peaks are observed at 350 (on the shoulder of the A_1 mode), 302, 320, and 458 cm^{-1}, respectively [30,31]. However, no secondary phase of $Cu_{2-x}S$ is seen in the Raman spectra of the Cu-poor sample in Fig. 3(c) either before or after the KCN etching. Even from the spectra of the Cu-rich sample (Fig. 3(d)) where the $Cu_{2-x}S$ peak is strong, the intensity of the $Cu_{2-x}S$ peak that is observed only before the etching is much weaker than that for the sample excited at 488 nm (2.54 eV), as shown in Fig. 3(b). From this observation, we can estimate the stoichiometry of $Cu_{2-x}S$ to be $Cu_{2-x}S$ ($x = 1$) as follows: The band gap of $Cu_{2-x}S$ depends on x, and it is ∼2.5 eV when $x = 1$ (CuS) [29]. Considering that the $Cu_{2-x}S$ peak is strong

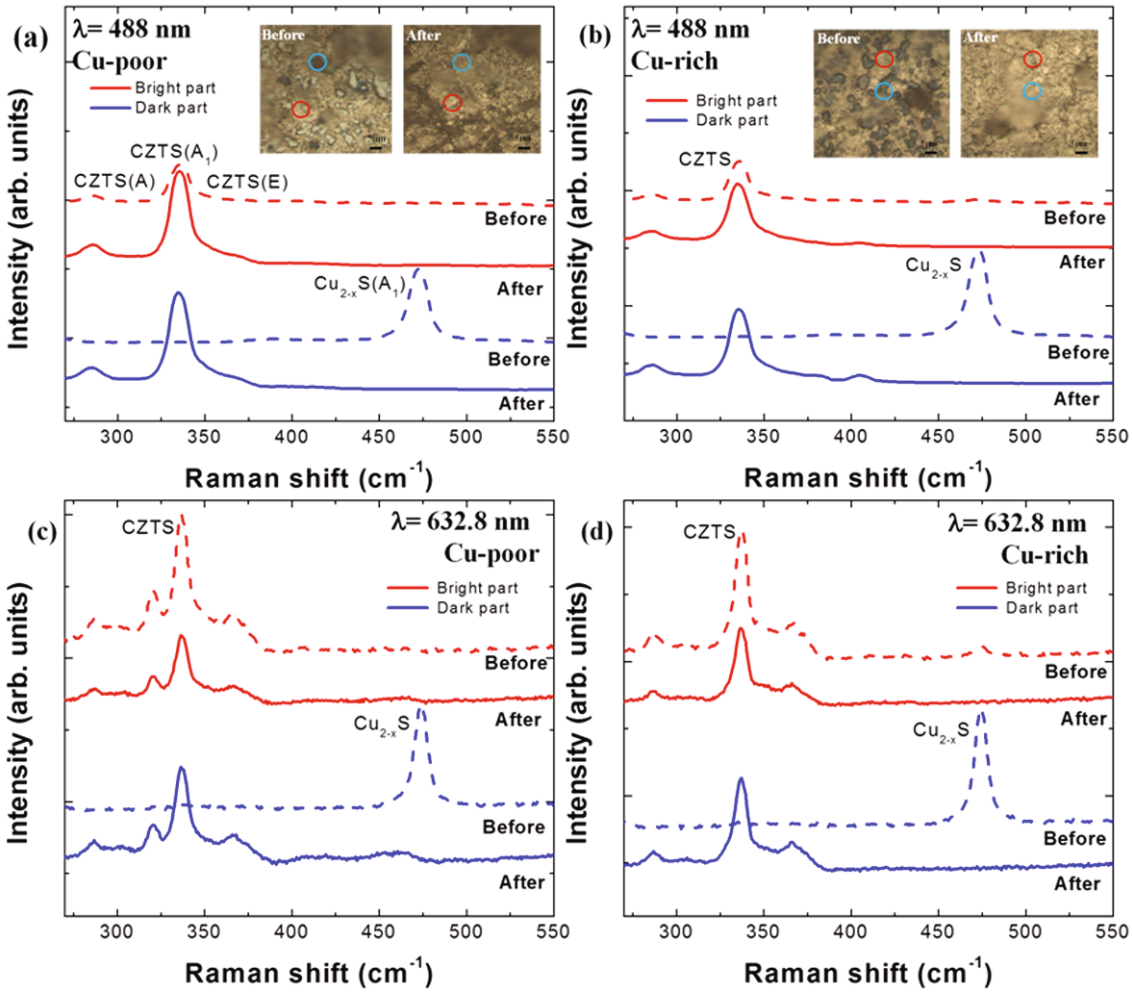

Fig. 4. (Color online) Optical images (×100 lens) and corresponding micro-Raman spectroscopy results for CZTS thin films before KCN-etching and after KCN-etching by using a 488-nm laser and a 632.8-nm laser.

only when the sample is excited at 2.54-eV (488 nm) and not at 1.96-eV (632.8 nm), the relevant energy scale that can cause a resonance (selective enhancement) is ∼2.5 eV, which is the band gap of $Cu_{2-x}S$ ($x = 1$). The second phase of $Cu_{2-x}S$ is found to have been removed by the KCN etching for both excitations of 2.54 eV (488 nm) and 1.96 eV (632.8 nm).

Figure 4 shows optical images and the micro-Raman spectra of CZTS thin films before and after the KCN etching of Cu-poor and Cu-rich samples. In the optical images of the Cu-poor and the Cu-rich samples before etching, as shown in Figs. 4(a) and (b), bright and dark parts are observed and are clearly distinguishable. However, the dark parts are seen to mostly disappear from the optical images after the etching. To compare the local effect of the KCN etching, we measured micro-Raman spectra at the same places of each sample before and after the etching. From Figs. 4(a) and (c), only the CZTS peaks are observed at the bright part of Cu-poor samples, regardless of etching. On the other hand, only the $Cu_{2-x}S$ peak at 473 cm^{-1} is clearly observed at the dark part of Cu poor samples before etching but it disappears and CZTS peaks are observed after etching. In the bright part of the Cu-rich samples (Figs. 4(b) and (d)), the intensity of the $Cu_{2-x}S$ peak is very weak before etching and becomes zero after etching. In the dark part of the Cu-rich samples, however, the same trend of $Cu_{2-x}S$ observation as in the Cu-poor samples is observed. From this observation, we can conclude that the most of the secondary phase of $Cu_{2-x}S$ is concentrated in the dark part. Removal of the $Cu_{2-x}S$ by KCN etching is also confirmed by the micro-Raman measurements, where results are completely consistent with those of macro-Raman measurements.

Table 2 shows the intensity ratio of the $Cu_{2-x}S$ peak at 473 cm^{-1} to the CZTS peak at 337 cm^{-1}, $I_{Cu2-x}S/I_{CZTS}$, for the Raman spectra measured from the Cu-rich samples before etching because the secondary phase of $Cu_{2-x}S$ disappears after the KCN etching. In the macro-Raman analysis, the intensity ratios are about 1.1 and 0.6 for 488-nm and 632.8-nm excitations, respectively, and in the micro-Raman analysis, the

Table 2. Intensity ratio of the main peak of $Cu_{2-x}S$ (∼473 cm^{-1}) to that of CZTS (∼337 cm^{-1}), $I_{Cu2-x}S/I_{CZTS}$, for Cu-rich samples before KCN etching-sample.

$I_{Cu2-x}S/I_{CZTS}$	Wavelength (nm)	
	488	632.8
Macro Raman (d = 100 μm)	1.1	0.6
Macro Raman (d = 1 μm)	2.0	0.9

corresponding ratios are about 2.0 and 0.9. The penetration depths for 488-nm and 632.8-nm are 140 nm and 170 nm, respectively [30], and the focused spot size of the 488-nm laser is smaller than that of the 632.8-nm laser. Interestingly, the intensity ratio $I_{Cu2-x}S/I_{CZTS}$ for excitation at 488 nm (2.54 eV) is always larger than that for excitation at 632.8-nm (1.96 eV) due to the resonance effect.

IV. CONCLUSION

Using different excitation wavelengths of 488 nm (2.54 eV) and 632.8 nm (1.96 eV) for the Raman scattering experiment, we studied the secondary phase of CZTS thin films grown by using the electroplating method. We observed a resonance effect of the secondary phase of $Cu_{2-x}S$, from which we could estimate the stoichiometry of the phase as $Cu_{2-x}S$ ($x = 1$). We could also find the local distribution of the $Cu_{2-x}S$ phase by using micro Raman spectroscopy. Our observation clearly shows that the second phase of $Cu_{2-x}S$ can be removed by KCN etching.

ACKNOWLEDGMENTS

The work is supported by National Research Foundation of Korea (NRF) grants funded by the Korean government's Ministry of Science, ICT and Future Planning (2008-0062237) and a New & Renewable Energy Technology Development Program of the Korea Institute of Energy Technology Evaluation and Planning (KETEP) grant funded by the Korea government's Ministry of Knowledge Economy (no. 20113020010040).

REFERENCES

[1] W. Wang, M. T. Winkler, O. Gunawan, T. Gokmen, T. K. Todorov, Y. Zhu and D. B. Mitzi, Adv. Energy Mater. (2013), [DOI: 10.1002/aenm.201301465].
[2] D. B. Mitzi, O. Gunawan, T. K. Todorov, K. Wang and S. Guha, Sol. Energy Mater. Sol. Cells **95**, 1421 (2011).
[3] B. Shin, O. Gunawan, Y. Zhu, N. A. Bojarczuk, S. J. Chey and S. Guha, Prog. Photovolt: Res. Appl. **21**, 72 (2011).
[4] P. Jackson, D. Hariskos, E. Lotter, S. Paetel, R. Wuerz, R. Menner, W. Wischmann and M. Powalla, Prog. Photovolt: Res. Appl. **19**, 894 (2011).
[5] K. Oishi *et al.*, Thin Solid Films **517**, 1449 (2008).
[6] H. Katagiri, K. Jimbo, S. Yamada, T. Kamimura, W. S. Maw, T. Fukano, T. Ito and T. Motohiro, Appl. Phys. Express **1**, 041201 (2008).
[7] Y. B. K. Kumar, G. S. Babu, P. U. Bhaskar and V. S. Raja, Sol. Energy Mater. Sol. Cells **93**, 1230 (2009).
[8] K. Moriya, K. Tanaka and H. Uchiki, Jpn. J. Appl. Phys. **47**, 602 (2008).
[9] J. J. Scrag, P. J. Dale and L. M. Peter, Thin Solid Films **517**, 2481 (2009).
[10] J. Lehner, M. Ganchev, M. Loorits, N. Revathi, T. Raadik, J. Raudoja, M. Grossberg, E. Mellikov and O. Volobujeva, J. Crystal Growth **380**, 236 (2013).
[11] S. Ahmed, K. B. Reuter, O. Gunawan, L. Guo, L. T. Romankiw and H. Deligianni, Adv. Energy Mater. **2**, 253 (2012).
[12] B. S. Pawar, S. M. Pawar, K. V. Gurav, S. W. Shin, J. Y. Lee, S. S. Kolekar and J. H. Kim, ISRN Renewable Energy **2011**, 934575 (2011).
[13] M. Valdes, M. Modibedi, M. Mathe, T. Hillie and M. Vazque, Electrochimica Acta (in press).
[14] P. A. Fernandes, P. M. P. Salomé, A. F. Sartori, J. Malaquias, A. F. da Cunha, B.-A. Schubert, J. C. González and G. M. Ribeiro, Sol. Energy Mater. Sol. Cells **115**, 157 (2013).
[15] M. Bär, B.-A. Schubert, B. Marsen, S. Krause, S. Pookpanratana, T. Unold, L. Weinhardt, C. Heske and H.-W. Schock, Appl. Phys. Lett. **99**, 152111 (2011).
[16] K. D. Lee, S.-W. Seo, D.-K. Lee, H. Kim, J. Jeong, M. J. Ko, B. S. Kim, D. H. Kim and J. Y. Kim, Thin Solid Films **546**, 294 (2013).
[17] A. Weber, R. Mainz, T. Unold, S. Schorr and H.-W. Schock, Phys. Status Solidi C **6**, 1245 (2009).
[18] H. Araki, Y. Kubo, K. Jimbo, W. S. Maw, H. Katagiri, M. Yamazaki, K. Oishi and A. Takeuchi, Phys. Status Solidi C **6**, 1266 (2009).
[19] K. D. Lee, S.-W. Seo, D.-K. Lee, H. Kim, M. J. Ko, B. S. Kim, D. H. Kim and J. Y. Kim, ECS Trans. **50**, 101 (2013).
[20] A. Rubo, R. Kellens, J. Reddy, N. Steier and W. Hasenpusch, *Ullmann's Encyclopedia of Industrial Chemistry* (Wiley-VCH, Weinheim, 2006).
[21] P. Patnaik, *Handbook of Inorganic Chemicals* (McGraw-Hill, New York, 2002).
[22] M. Bär *et al.*, Phys. Rev. B **84**, 035308 (2011).
[23] K. Timmo, M. Altosaar, J. Raudoja, M. Grossberg, M. Danilson, O. Volobujeva and E. Mellikov, *Proceeding of the 35th IEEE Photovoltaic Specialists Conference* (Honolulu, HI, 2010), p. 1982.
[24] J. Park, M. Song, W. M. Jung, W. Y. Lee, H. Kim, Y. Kim, C. Hwang and I.-W. Shim, Dalton Trans. **42**, 10545 (2013).
[25] B.-A. Schubert, B. Marsen, S. Cinque, T. Unold, R. Klenk, S. Schorr and H.-W. Schock, Prog. Photovolt: Res. Appl. **19**, 93 (2011).

[26] M. Himmrich and H. Haeuseler, Spectrochem. Acta **47**, 933 (1991).
[27] D. Dumcenco and Y. S. Huang, Opt. Mater. **35**, 419 (2013).
[28] P. A. Fesnades, P. M. P. Salome and A. F. da Cunha, J. Alloys Comp. **509**, 7600 (2011).
[29] A. Phurugrant, T. Thongtem and S. Thongtem, Chalcogenide Letters **8**, 291 (2011).
[30] X. Lin, J. Kavalakkatt, K. Kornhuber, S. Levcenko, M. Ch. Lux-Steiner and A. Ennaoui, Thin Solid Films **535**, 10 (2013).
[31] H. Li, Q. Zhang, C. C. R. Yap, B. K. Tay, T. H. T. Edwin, A. Olivier and D. Baillargeat, Adv. Funct. Mater. **22**, 1385 (2012)